

Osteoarticular tuberculosis in children. A fast reappearing disease diagnosed by ^{18}F -FDG PET/CT and other modalities. The cover page of Nicholas Andry booklet *L' Orthopedie*

Yuxiao Xia¹ MD,
Nikitas Papadopoulos² MD,
Yue Chen¹ MD
Yanhong Zhao¹ MD

Abstract

Osteoarticular tuberculosis (OAT) is not uncommon in children. Early diagnosis and treatment are essential to avoid ultimately long-term disabilities. Nicolas Andry (1658-1742) gave for the first time the name of the specialty of Orthopedics (*L' Orthopedie*) and its symbol of the crooked tree, in a paper in which he suggested how to avoid and to treat rachitis in children. We review the correlative-imaging findings and provide insights regarding the strengths and limitations of the conventional imaging modalities and those of nuclear medicine for the diagnosis of OAT and its differential diagnosis from other diseases.

Hell J Nucl Med 2018; 21(3): 205-212

Epub ahead of print: 10 November 2018

Published online: 5 December 2018

1. Department of Nuclear Medicine,
The Affiliated Hospital,
Southwest Medical University,
Luzhou, Sichuan, PR China.
2. Department of Nuclear Medicine,
Theageneio Anticancer Hospital,
Thessaloniki, Greece

Keywords: Osteoarticular
tuberculosis - Children
- Radiograph - MRI - SPET - PET/CT

Corresponding author:

Yue Chen, MD
Department of Nuclear Medicine,
The Affiliated Hospital,
Southwest Medical University,
No 15 TaiPing St, Jiangyang
District, Luzhou, Sichuan, PR
China, 646000
chenyue5523@126.com

Received:

18 July 2018

Accepted revised:

18 September 2018

Introduction

Tuberculosis (TB) was endemic in animals from the Paleolithic Age, about 2-3 million years ago, long before affecting humans [1, 2]. Other researchers reported that TB in men was present at the Middle Neolithic Age, 6,500 years ago [3]. Nicolas Andry (1658-1742) gave for the first time the name of Orthopedics (*L' Orthopedie*) as a new specialty and its symbol of the crooked tree (Figure 1). In his paper he suggested how to avoid and to treat rachitis in children [4]. The disease is due to Koch's bacillus or mycobacterium of tuberculosis and can be transmitted even by air quite easily [5]. Children present a much greater risk than adults, often through exposure to adults infected with the bacillus [6].

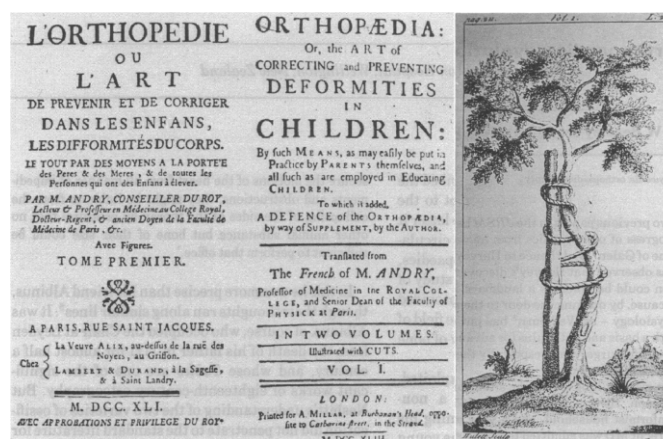


Figure 1. Nicholas Andry (1658-1742) gave orthopaedics its name and the symbol of the crooked tree.

Today, TB is one of the top 10 causes of death worldwide. World Health Organization (WHO) estimated that 10.4 million people fell ill with TB and 1.7 million died from the disease in 2016. Over 95% of TB deaths occurred in low-and middle-income countries, mainly in India, followed by Indonesia, China, Philippines, Pakistan, Nigeria, and South Africa. Pigrau-Serrallach and Rodríguez-Pardo (2013) [2] found that in developed countries, the proportion of bone and joint TB in children was 10%-15%. In less developed countries in Asia and Africa, this proportion is 15%-20%, and indicates the distribution of the disease associated with the acquired immune deficiency syndrome (AIDS) epidemic and the low level of economic activity, immigration [7-9]. Another study [10] has also found that TB was associated with a growing number of immunocompromised patients

and emergence of multidrug-resistant (MDR) strains of mycobacterium TB. According to WHO (2016), an estimated 1 million children became ill with TB and 250000 children died of TB, including children with HIV associated with the disease.

Extrapulmonary tuberculosis (EPTB) is common in children and its clinical presentation varies with age. Around 20% of all mycobacterial infections in children are EPTB [11], including osteoarticular TB. Osteoarticular TB has an equal incidence between the sexes [12]. Bone and joint involvement is considered the third most common type of EPTB following thoracic and lymph node TB [1, 6].

The most common manifestations of osteoarticular TB in children are spondylitis, arthritis and osteomyelitis. Spinal TB, known as 'Pott's Disease', is one of the most common osteoarticular TB, accounting for about 50% of skeletal TB cases which most likely occurs in the thoracic vertebrae causing rachitis [13-16]. The Rajasekaran study (1998) [17] found that the number of segments involved in pediatric spinal TB was 1.9 times more than that of adults. Pediatric vertebrae are more likely to be damaged than adult vertebrae because they consist primarily of cartilage. Spinal TB causes destruction of vertebral bodies leading to typical spinal deformity and possibly paralysis. If rachitis is left untreated, kyphosis is formed which will continue to grow as the child grows up [17, 18]. Deformity may be further aggravated in time even after TB is cured [19]. This deformity affects not only the spine, but also the cardiopulmonary function and may cause spinal cord compression. Approximately 20% of patients with spinal TB undergo surgery [13]. Early diagnosis and appropriate therapy are crucial for the successful treatment of this disease [2, 19].

Imaging methods

It is difficult to get samples from the lesion of bones for histopathologic examination especially in children who usually show poor compliance [14]. Diagnosis is often clinically suspected.

In a study by Su-Ting Chen et al. (2015) [14], 108 out of 113 patients with osteoarticular TB were empirically diagnosed by imaging modalities. The existing imaging modalities are as ultrasound, X-rays, computed tomography, magnetic resonance imaging (MRI) and nuclear medicine techniques. Nuclear medicine techniques include single photon emission tomography (SPET) and fluorine-18-fluoro deoxy glucose positron emission tomography/computed tomography (^{18}F -FDG PET/CT) and ^{18}F -sodium fluoride PET/CT (^{18}F -NaF PET/CT) and play an important role in diagnosing and evaluating the severity and therapeutic response of osteoarticular TB.

Conventional imaging

X-rays radiographs remains the initial modality for mass screening purposes. The most frequent radiological findings in osteoarticular TB are: bone destruction, cold abscesses and hypertrophic articular membrane [6]. Furthermore, narrowing of the intervertebral space (Figure 2) and the degree of kyphosis (Figure 3). In practice, distinguishing

TB spondylitis from pyogenic spondylitis on plain radiographs is usually not possible. The earliest sign diagnosed by X-rays may be demineralization of the endplates of the vertebrae with resorption and loss of 30% of bone mineral [7]. With further progression of the disease, radiographs will show progressive vertebral collapse with anterior wedging and varying degrees of kyphosis [7, 20, 21]. Rajasekaran et al. (2001) [22] found that some additional signs appeared during the course of the spinal TB on the radiographs, like dislocation of the facet joints (Figure 2A), posterior retropulsion of the infected vertebral segments (Figure 2B), lateral translation of the vertebral column in the anteroposterior view (Figure 2C) and toppling of the superior vertebra (Figure 2D). These signs occur in the early stages of the disease, even in the active period. One can assess the risk of kyphosis in children through the features presented on the X-rays films. The presence of two or more signs is a reliable predictor of patient's spine deformity. For deformities exceeding 30 or even 60 degrees surgery is recommended in these cases [22]. Paravertebral abscess can be seen in the late stage of the disease on X-rays plain films [2]. The anterior type of the vertebrae is more common in the pediatric spinal TB and in such cases a globular or fusiform radiodense shadow is visible on plain radiographs. Long standing abscesses may produce a scalloped appearance called "the aneurysmal phenomenon", which is due to concave erosions around the anterior margins of the vertebral bodies.

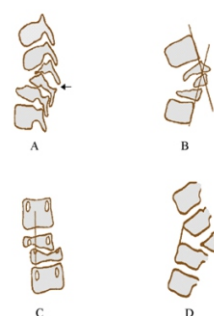


Figure 2. Radiological signs of "spine at risk of kyphosis".



Figure 3. A 6 years old girl with spine TB. Radiograph shows narrowing of the T10-T11 intervertebral disc space (arrow).



Figure 4. A 10 years old boy with spine tuberculosis. Preoperative radiological showed destructive segments located at T11-T12 vertebrae, with a kyphosis.

Peri-articular osteoporosis, peripherally located osseous erosion, and progressive decrease in the joint space suggest the diagnosis of tuberculous arthritis and are popularly referred to as the 'Phemister triad'. The joint space gradually decreases as the disease progresses. However, the destruction of cartilage may not be noted on X-rays plain films.

Tuberculous osteomyelitis is most often involved in the skull vault, hands, feet and ribs [23]. The multiple sites involved are often seen in children, but are more limited to single bones in adults. On radiographs, soft-tissue swelling and osteoporosis are seen in all forms of tuberculous osteomyelitis. These lesions have different imaging findings: cystic, focal erosions, infiltrative and dactylitis and the cystic manifestation in children are more than that in adults, showing radiolucent prototype or oval lesions, with visible marginal sclerosis in some cases. Sometimes the expansion of the bones and honeycombs will be seen (Figure 5). These cystic lesions may cross the epiphyseal plate to involve epiphysis. The radiographs show that these lesions appear as cyst-like cavities with enlarged diaphyses. However, the relatively low resolution of X-rays plain films, overlapping tissues and organs and image artifacts, may diminish the diagnostic value of the image showed. Therefore, other imaging examinations should be supplemented.

Compared with plain radiographs, CT provides better details of irregular lytic and sclerotic lesions, disc collapse and disruption of bone circumference (Figure 6B, C) and also better define the shape and possible calcification of soft tissue abscesses (Figure 6A) [7, 24]. Furthermore, CT can better show Pott's disease by identifying sequestrums, perilesional sclerosis and epidural or soft tissue abscesses [24], especially in areas that are difficult to assess on radiographs such as posterior lesions [25]. Patterns of bone destruction (fragmentary, sclerotic, osteolytic, and subperiosteal) can also be well observed on CT [7, 24]. Patients with suspected lung or abdominal TB often undergo CT examinations and thus detect clinically unsuspected, skeletal TB [24]. In addition, CT is ideal for guiding a percutaneous diagnostic biopsy. It has been reported that CT in cases of spinal infections can diagnose TB in 77% [7, 24, 26-28]. However, the role of CT in de-

fining the epidural space distention due to the disease and its effect on the neural structure is less accurate. The CT findings related to soft tissue masses, the intervertebral discs and spinal cord were not as accurate as those of MRI [24].

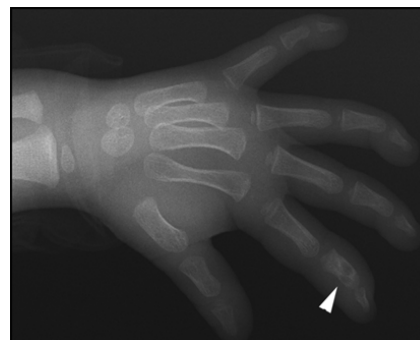


Figure 5. A 3 years old boy with phalangeal TB. Palm radiograph shows cystic low-density shadow in the bone marrow cavity of the middle phalanx of the index finger (arrow).



Figure 6. Transaxial CT imaging of patients with known osteoarticular TB. A, A 17 years old boy with cold abscess. Axial CT finds calcification of the right psoas major abscess (arrow). B, A 6 years old girl with TB. The eroded T11 vertebra and paravertebral abscess is seen on the CT image (arrow). C, A 10 years old boy with TB involving the right acetabulum. The axial CT image showed irregular lytic lesions and sclerosis (arrow).

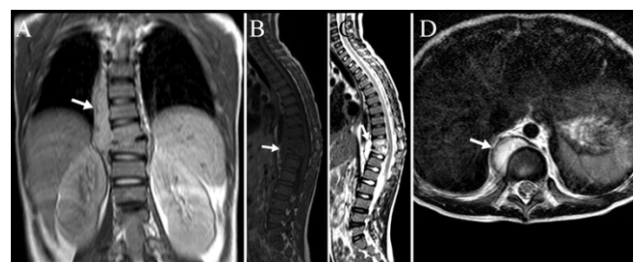


Figure 7. A 6 years old girl with spine TB. Images from MRI (T1, A-B and T2, C-D) showing destructive segments located at T10-T11 vertebrae and showing paravertebral collection extending from T7-T11 (arrow).

Magnetic resonance imaging can give us useful images without any ionizing radiation to patients, which is important in children and can evaluate bone marrow soft tissue involvement at the early stage of the disease. Vertebral collapse and paravertebral and epidural abscess, as well as the varying degrees of epidural compression, are best evaluated using MRI (Figures 7, 8). Magnetic resonance imaging is the

most sensitive for early diagnosis and follow-up of spinal TB [29]. The earliest sign for TB is marrow edema, which is seen as a hyperintense signal on T2 and short-tau inversion recovery (STIR) images. Changes in spinal TB are detected 4-6 months earlier by MRI than by conventional methods [30]. These changes include the destruction of the vertebra and the relative preservation of the intervertebral disc [2, 25, 31]. Chandrasekhar et al. (2013) [32] have suggested a novel MRI scoring system that tests eight parameters including T1 hypo intensity, T2 hyper intensity, disc involvement, epiphyseal involvement, pedicle involvement, paraspinal extension, anterior subligamentous extension and no spinous process involvement, and it was noted that score ≥ 6 favored a tuberculous pathology. Sureka et al. (2013) [33] reported that in MRI the involvement of the costovertebral joints and the posterior elements with intact low-signal cortical outline, suggested the possibility of spinal TB. Children with TB spondylitis more frequently than adults, showed in the intervertebral disc hypointense signal on T2-W images [34]. As the disease progresses, MRI shows loss of definition of the endplates and the adjacent vertebral bodies, with hypointense signal on T1 and hyperintense signal on T2 and STIR images. Spinal deformity can occur several months to years after the lesions heal, and glial cell proliferation, severe cord atrophy, syringohydromyelia and peridural contractile scars can be detected by MRI [35].

Magnetic resonance imaging in TB arthritis or osteomyelitis, often shows marrow changes, synovitis, joint effusion, pannus, tenosynovitis, bursitis, periarticular inflammation, cartilage and bone erosion (Figure 9). Gradient-echo sequence plays an important role in the evaluation of cartilage involvement [30]. These changes are usually hypointense signal in T1-W sequence and hyperintense signal in T2-W sequence. However, the imaging findings of TB arthritis are nonspecific on MRI. Suppurative and juvenile idiopathic arthritis may have similar characteristics.

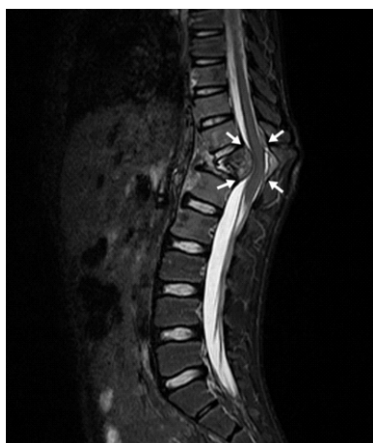


Figure 8. A 10 years old boy with spine TB. Sagittal T2-weighted MRI images showed epidural and paravertebral abscess formation, and spinal cord compression (arrow).

Ultrasonography can detect soft-tissue extension of the skeletal lesions and is widely used in guided needle aspiration or biopsy for early histopathological diagnosis [9, 25]. Unenhanced MRI does not necessarily differentiate synovial

thickening from effusion, but an ultrasound can help to differentiate them, with the former being anechoic and the latter being hypoechoic. In experienced hands, bone destruction (hyperechoic cortical with irregular bone destruction), abscess (the turbid liquid in and around the area of bone destruction), sequestrum formation (patchy and punctate strong echo), joint effusion (echo-free zone around the joint), soft-tissue swelling (muscles around the lesions with echo reduction), periosteal elevation (complete continuous echo on the surface of the cortical bone), destruction of epiphysis and epiphyseal cartilage (normal hypoechoic to echoless epiphyseal cartilage with blur boundaries and increased echo) and blood flow signals can be seen on ultrasound images of children with osteoarticular TB. Ultrasound with high-frequency transducers can provide invaluable information about the synovium, tendon sheaths, and bursal spaces [21, 25]. However, it is difficult to diagnose bone and joint TB only by ultrasonography.



Figure 9. A 17 years old boy with tibia TB. Magnetic resonance imaging shows a tubercle in the metaphysis of the left tibia, involving the epiphysis, which is about 1.3cm×2.0cm in its largest dimension (arrow).

Nuclear medicine imaging

Nuclear medicine imaging technology allows for the most accurate correlation of anatomical and metabolic information, enabling the fusion of anatomical and functional images. Fusion imaging contributes to early detection and evaluation of diseases involvement. Anatomical imaging can evaluate the structural changes associated with infection while functional imaging can demonstrate early functional impairment secondary to infectious process. Single photon emission computed tomography/CT, PET/CT as emission computed tomography (ECT) contribute to early diagnosis and treatment response evaluation of osteoarticular TB [36].

Single photon emission tomography-bone-targeting radiopharmaceuticals are analogs of calcium, hydroxyl groups or phosphates. The most commonly used radiopharmaceuticals are ^{99m}Tc -labeled diphosphonates for imaging osteoblastic activity, such as methylene diphosphonate (MDP) [37]. Compared with planar ^{99m}Tc -MDP whole-body bone scintigraphy, SPET/CT imaging allows three-dimensional localization of tracer activity to bone lesions (Figure 10) and is useful for differentiating soft tissue from bone infections, for assessing sites of suspicious bone infection with structural alterations and can observe the extent of the lesion at

complex anatomical sites [37]. In addition, the early and delayed ^{99m}Tc -MDP SPET/CT imaging can differentiate other disease like rheumatoid arthritis and osteoarthritis [38]. Other radiopharmaceuticals used for the diagnosis of skeletal infections are ^{99m}Tc -PYP, ^{99m}Tc -HMDP and ^{99m}Tc -HEDP. A study [39] suggested that SPET/CT with ^{99m}Tc -EDDA-HYNIC-TOC or ^{111}In -DTPA-octreotide can differentiate bone TB from systemic granulomatous infections but not from other bacterial infections.

Ethambutol is one of the first-line treatments for TB. Kartamihardja et al. (2018) [40] showed that ^{99m}Tc -ethambutol is a useful radiopharmaceutical to detect and localize both intra- and extra-pulmonary TB with minimal or no side-effects while is safe to be performed even in pediatric patients.

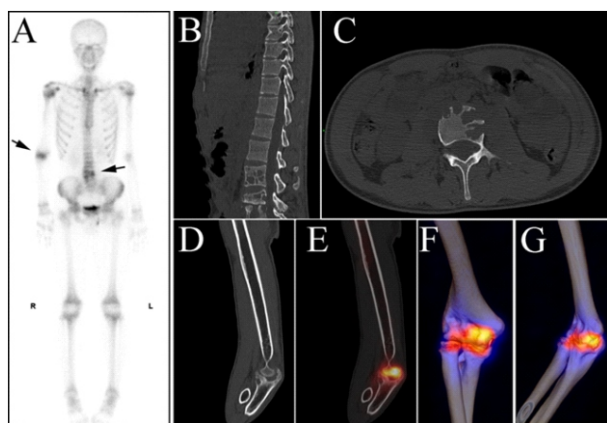


Figure 10. Single photon emission tomography/CT imaging (with ^{99m}Tc -MDP) of patients with osteoarticular TB. A-G, A 17 years old boy with spinal and elbow TB. The anterior maximum intensity projection images (A) showed abnormal activity at the L2-L5 vertebrae and the right elbow joint. (B, C and D) CT images showed bone destruction in these sites. The SPET/CT (E) and 3D-SPET (F and G) images not only showed the metabolic status of the lesions, but also determined the location of the lesions more clearly and intuitively.

Children who use SPET/CT have lagged behind adults for fear that CT components may increase the dose of radiation burden in children [41]. Therefore, SPET/CT scans should be tailored to every child examined to ensure compliance with the ALARA (as low as reasonably achievable) principle for radiation protection.

Fluorine-18-FDG PET/CT shows superior image resolution [42,43]. Recent advances in PET imaging systems have increased the ability to visualize and quantify small concentrations of PET tracers for patients thus using low-dose radiation [44]. Since TB in children involves the extremities more often than in adults and also more extensive disease, whole-body imaging is essential in suspected TB cases [2, 21, 45, 46]. It can also assess and stage pulmonary and extrapulmonary TB simultaneously, saving time and cost [47, 48]. Albano et al. (2017) [49] reported that ^{18}F -FDG PET/CT revealed incidentally unilateral TB sacroiliitis. Furthermore, ^{18}F -FDG PET/CT can differentiate active from latent TB [50-52], with high sensitivity while high image quality negative studies largely exclude active disease. A recent study found that ^{18}F -FDG PET/CT was superior to MRI in differentiating TB and suppurative spondylitis [52, 53]. The SUV level of ^{18}F -FDG PET in TB spon-

dylodiscitis was higher than that in pyogenic spondylodiscitis [54]. However, some scholars still do not believe that ^{18}F -FDG PET/CT is able to clearly distinguish granulomatous disease from other diseases, such as bone metastases or suppurative osteomyelitis, based on standardized uptake values (SUVmax) [52, 55]. Dual-time-point imaging (DTPI) has been used to distinguish benign from malignant processes. Although some reports indicate that DTPI may help identify TB [56], its value remains controversial [52]. In recent years, three-dimensional reconstruction technology has also been gradually applied to nuclear medicine imaging. 3D PET/CT and 3D SPET/CT images are helpful in locating lesions even by complex anatomic sites [57].

In addition, ^{18}F -FDG PET/CT has been used for the guidance of biopsy, the development of surgical plan, and the evaluation of follow-up [51, 54, 58, 59]. One of the main advantages of PET is its ability to semi-quantify ^{18}F -FDG uptake and assesses the early response to treatment in EPTB and especially in TB abscesses while the radiologic characteristics may remain unchanged [47, 50, 52, 60-62]. During one month follow-up, Bassetti et al. (2017) [54] showed an average reduction of 48% in SUV of tuberculous spondylodiscitis after anti-tuberculosis treatment. In developing countries, TB multi-drug-resistant (MDR) and extensively drug-resistant (XDR-TB) often need monitoring therapy.

Some studies [58, 63] have demonstrated that the size of some bacillus-negative tuberculomas may remain unchanged or even increase during anti-TB treatment. Fluorine-18-FDG PET/CT imaging can be useful in this situation. If the lesion activity increases, the tuberculoma is likely to be active and the previous treatment protocol should be discontinued and changed, and surgery should be performed if necessary. If the lesion is significantly reduced or there is residual faint activity, current treatment should be continued [63, 64].

In general, after 3 to 9 months of continuous treatment, ^{18}F -FDG PET/CT may show an objective response to the treatment [52]. In addition, ^{18}F -FDG PET/CT was proposed as a surrogate end point for new drug trials and a marker of disease status in patients with HIV and TB co-infections [5, 52]. Future developments in nuclear medicine in the diagnosis of bone and joint TB may include anti-TB-related tracers and improvements in the semi-quantification of osteoarticular TB lesions [52].

Sodium fluoride labeled with fluorine-18 PET/CT

In 1962, Blau first proposed ^{18}F -NaF as a bone scanning agent, yet its clinical use was restricted by the fact that gamma camera scanners were unavailable at that time. In the late 1990s, with the advent of the hybrid PET/CT camera, the interest in using ^{18}F -NaF was rekindled [65].

Sodium fluoride labeled with fluorine-18 is an excellent bone-seeking agent, which binds to the bone at the site of bone formation or remodeling [66]. The bone uptake of ^{18}F -NaF was twice as much as that of ^{99m}Tc -MDP, and was removed more rapidly by soft tissues, thus shortening the examination time and increasing bone-background ratio of ^{18}F ions, thus improving accuracy of bone lesions detection [67]. The favorable kinetics of ^{18}F -NaF make it an accurate imaging

agent for bone blood flow and metabolism. The superior image contrast and high spatial resolution of ^{18}F -NaF PET/CT provide greater anatomic localization of osseous lesions and have been used in various types of bone disorders, including bone and joint TB (Figure 11). Several other studies [68, 69] has shown that ^{18}F -NaF PET/CT have a higher negative predictive value compared with $^{99\text{mTc}}$ -MDP SPET and planar $^{99\text{mTc}}$ -MDP. In the process of inflammation, the early-phase images of ^{18}F -NaF PET/CT demonstrated that the uptake of the radioactive tracer increased, as also the information obtained from the perfusion and blood pool phase of the three-phase bone scan, suggesting that ^{18}F -NaF PET/CT early-phase scan may replace three-phase bone scan [70, 71]. Beyond that, ^{18}F -NaF PET/CT scans have the ability to evaluate semi-quantitative parameters such as SUV and has the potential for monitoring treatment response in patients with bone TB.

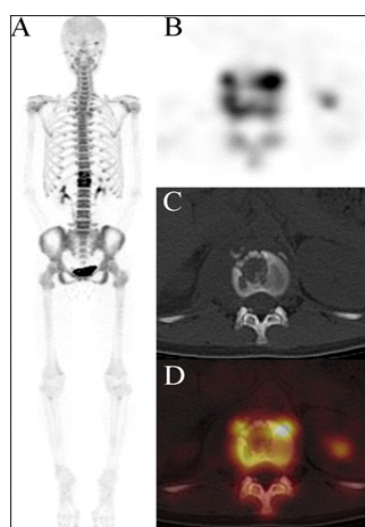


Figure 11. Fluorine-18-NaF PET/CT imaging of patients with spine TB. (A) A 17 years old girl with spine TB. Maximum intensity projection image showed increased ^{18}F -NaF uptake in T12-L1 vertebrae. (B, C and D) The axial images of PET/CT demonstrated that the bone structure was disordered with some osteolytic bony destruction and abnormal activity. Maximum standardized uptake value (SUVmax) was 24.5.

Sodium fluoride labeled with fluorine-18 is administered in smaller doses, so that the total actual radiation absorbed dose was almost comparable with that of $^{99\text{mTc}}$ -labeled conventional bone imaging agents. In addition, ^{18}F -NaF has a low affinity to proteins, fast clearance from blood and excellent extraction from bones which make ^{18}F -NaF an excellent bone imaging agent [72].

It is also important to recognize the limitations of ^{18}F -NaF PET/CT, including high cost and that it is non-specific for the diagnosis of tuberculous osteoarthropathy [73] because tumors, traumas and other bone malformations such as fibrous dysplasia and Paget's disease. On the other hand, PET/CT imaging, although quite useful to diagnose osteoarthral TB [74] is also expensive.

In conclusion, pediatric osteoarthral TB remains a diagnostic problem in our days. Early diagnosis and treatment are essential to avoid skeletal deformities and ultimately

long-term functional disabilities [75, 76]. Radiography can be used as initial screening. Computed tomography provides details of skeletal lesions, more effectively defining the calcification of soft tissue abscesses. Magnetic resonance imaging is the best modality for evaluating TB spondylitis. It helps to determine the presence of epidural components and cord compression. Ultrasonography is usually helpful in identifying abscesses, joint effusions and is widely used in guiding needle aspiration. Nuclear medicine techniques play an important role in the detection of TB lesions, disease activity and disease stage, disease complications identification of dynamic and latent disease and of potential biopsy targets [77].

Bibliography

1. Plesea IE, Anusca DN, Procopie I et al. The clinical-morphological profile of bone and joints tuberculosis-our experience in relation to literature data. *Rom J Morphol Embryol* 2017; 58: 887-907.
2. Pigrau-Serrallach C, Rodriguez-Pardo D. Bone and joint tuberculosis. *Eur Spine J* 2013; 22 Suppl 4: 556-66.
3. Sparacello VS, Roberts CA, Kerudin A et al. A 6500-year-old Middle Neolithic child from Pollera Cave (Liguria, Italy) with probable multifocal osteoarthral tuberculosis. *Int J Paleopathol* 2017; 17: 67-74.
4. Beasley AW. Orthopaedics: evolution of the specialty. *J Royal Soc Med* 1986; 79(6): 607-10 & Andry N. *Orthopaedia* (English translation). London: Millar, 1743.
5. Pelletier-Galarneau M, Martineau P, Zuckier LS et al. ^{18}F -FDG-PET/CT Imaging of Thoracic and Extrathoracic Tuberculosis in Children. *Semin Nucl Med* 2017; 47: 304-18.
6. Perez Duran MJ, Moreno Sanz-Gadea B, Del Rosal Raves T et al. Osteoarthral tuberculosis in paediatrics: A review of 20. years of cases in a tertiary hospital. *An Pediatr* 2017; 87: 291-2
7. Ansari S, Amanullah MF, Ahmad K et al. Pott's Spine: Diagnostic Imaging Modalities and Technology Advancements. *N Am J Med Sci* 2013; 5: 404-11.
8. Snene H, Berraies A, Hamdi B et al. Childhood tuberculosis: A descriptive study in a pneumo-pediatrics department in Tunisia. *Tunis Med* 2016; 94: 259-64.
9. Peghin M, Rodriguez-Pardo D, Sanchez-Montalva A et al. The changing epidemiology of spinal tuberculosis: the influence of international immigration in Catalonia, 1993-2014. *Epidemiol Infect* 2017; 145: 2152-60.
10. Firth GB, Lescheid J, Camacho M et al. Extraspinal osteoarthral multidrug-resistant tuberculosis in children: A case series. *S Afr Med J* 2017; 107: 983-6.
11. Le Roux P, Quinque K, Bonnel AS et al. Extra-pulmonary tuberculosis in childhood. *Arch Pediatr* 2005; 12 Suppl 2: S122-6.
12. Morris BS, Varma R, Garg A et al. Multifocal musculoskeletal tuberculosis in children: appearances on computed tomography. *Skeletal Radiol* 2002; 31: 1-8.
13. De la Garza Ramos R, Goodwin CR, Abu-Bonsrah N et al. The epidemiology of spinal tuberculosis in the United States: an analysis of 2002-2011 data. *J Neurosurg Spine* 2017; 26: 507-12.
14. Chen ST, Zhao LP, Dong WJ et al. The Clinical Features and Bacteriological Characterizations of Bone and Joint Tuberculosis in China. *Sci Rep* 2015; 5: 11084.
15. Marais S, Roos I, Mitha A et al. Spinal tuberculosis: Clinicoradiological findings in 274 patients. *Clin Infect Dis* 2018; 67(1): 89-98.
16. Varghese P, Abdul Jalal MJ, Kandathil JC et al. Spinal Intramedullary Tuberculosis. *Surg J* 2017; 3: e53-7.
17. Rajasekaran S, Shanmugasundaram TK, Prabhakar R et al. Tuberculous lesions of the lumbosacral region. A 15-year follow-up of patients treated by ambulant chemotherapy. *Spine* 1998; 23: 1163-7.
18. Jain AK, Dhammi IK, Jain S et al. Kyphosis in spinal tuberculosis - Prevention and correction. *Indian J Orthop* 2010; 44: 127-36.

19. Wong YW, Samartzis D, Cheung KMC et al. Tuberculosis of the spine with severe angular kyphosis: mean 34-year post-operative follow-up shows that prevention is better than salvage. *Bone Joint J* 2017; 99-B: 1381-8.
20. Desnos L, Kom-Tchameni R, Razafindrakoto H et al. Multifocal tuberculosis revealed by spinal tuberculosis in an eleven-year-old Guianese child. *Bull Soc Pathol Exot* 2017; 110: 234-7.
21. Bomanji JB, Gupta N, Gulati P et al. Imaging in tuberculosis. *Cold Spring Harb Perspect Med* 2015; 5(6): a017814.
22. Rajasekaran S. The natural history of post-tubercular kyphosis in children. Radiological signs which predict late increase in deformity. *J Bone Joint Surg Br* 2001; 83: 954-62.
23. Agarwal A, Gupta N, Mishra M et al. Primary epiphyseal and meta-epiphyseal tubercular osteomyelitis in children A series of 8 case. *Acta Orthop Belg* 2016; 82: 797-805.
24. Gupta P, Prakash M, Sharma N et al. Computed tomography detection of clinically unsuspected skeletal tuberculosis. *Clin Imaging* 2015; 39: 1056-60.
25. Teo HE, Peh WC. Skeletal tuberculosis in children. *Pediatr Radiol* 2004; 34: 853-60.
26. Joo EJ, Yeom JS, Ha YE et al. Diagnostic yield of computed tomography-guided bone biopsy and clinical outcomes of tuberculous and pyogenic spondylitis. *Korean J Intern Med* 2016; 31: 762-71.
27. Spira D, Germann T, Lehner B et al. CT-Guided Biopsy in Suspected Spondylodiscitis-The Association of Paravertebral Inflammation with Microbial Pathogen Detection. *PLoS One* 2016; 11: e0146399.
28. Zou DX, Zhou JL, Zhou XX et al. Clinical efficacy of CT-guided percutaneous huge ilio-psoas abscesses drainage combined with posterior approach surgery for the management of dorsal and lumbar spinal tuberculosis in adults. *Orthop Traumatol Surg Res* 2017; 103: 1251-5.
29. Singh R, Magu NK, Rohilla RK. Clinicoradiologic Profile of Involvement and Healing in Tuberculosis of the Spine. *Ann Med Health Sci Res* 2016; 6: 311-27.
30. Lalla R, Singh MK, Patil TB et al. MRI of the spinal tuberculoma, paravertebral tubercular abscess and pulmonary tuberculosis. *BMJ Case Rep* 2013; 2013.
31. Lee SW, Lee SH, Chung HW et al. Candida spondylitis: Comparison of MRI findings with bacterial and tuberculous causes. *Am J Roentgenol* 2013; 201: 872-7.
32. Chandrasekhar YB, Rajesh A, Purohit AK et al. Novel magnetic resonance imaging scoring system for diagnosis of spinal tuberculosis: A preliminary report. *J Neurosci Rural Pract* 2013; 4: 122-8.
33. Sureka J, Samuel S, Keshava SN et al. MRI in patients with tuberculous spondylitis presenting as vertebra plana: a retrospective analysis and review of literature. *Clin Radiol* 2013; 68: e36-42.
34. Andronikou S, Jadwat S, Douis H. Patterns of disease on MRI in 53 children with tuberculous spondylitis and the role of gadolinium. *Pediatr Radiol* 2002; 32: 798-805.
35. Thammaroj J, Kitkhuandee A, Sawanyawisuth K et al. MR findings in spinal tuberculosis in an endemic country. *J Med Imaging Radiat Oncol* 2014; 58: 267-76.
36. Gupta V. The menace of tuberculosis and the role of nuclear medicine in tackling it. Now its time to tighten the loose strings. *Hell J Nucl Med* 2009; 12(3): 214-7.
37. Thang SP, Tong AK, Lam WW et al. SPECT/CT in musculoskeletal infections. *Semin Musculoskelet Radiol* 2014; 18: 194-202.
38. Abdelhafez YG, Hagge RJ, Badawi RD et al. Early and Delayed ^{99m}Tc-MDP SPECT/CT Findings in Rheumatoid Arthritis and Osteoarthritis. *Clin Nucl Med* 2017; 42: e480-1.
39. Monteiro PHS, de Souza TF, Moretti ML et al. SPECT/CT with radiolabeled somatostatin analogues in the evaluation of systemic granulomatous infections. *Radiol Bras* 2017; 50: 378-82.
40. Kartamihardja AHS, Kurniawati Y, Gunawan R. Diagnostic value of ^{99m}Tc-ethambutol scintigraphy in tuberculosis: compared to microbiological and histopathological tests. *Ann Nucl Med* 2018; 32: 60-8.
41. Nadel HR. Bone scan update. *Semin Nucl Med* 2007; 37: 332-9.
42. Skoura E, Zumla A, Bomanji J. Imaging in tuberculosis. *Int J Infect Dis* 2015; 32: 87-93.
43. Kaya E, Halac M, Sönmezoglu K et al. ¹⁸F-FDG-PET/CT findings in a patient with tuberculosis Hodgkin's disease and lupus vulgaris. *Hell J Nucl Med* 2009; 12(3): 285-6.
44. Surti S. Update on time-of-flight PET imaging. *J Nucl Med* 2015; 56: 98-105.
45. Wang JH, Chi CY, Lin KH et al. Tuberculous arthritis-unexpected extrapulmonary tuberculosis detected by FDG PET/CT. *Clin Nucl Med* 2013; 38: e93-4.
46. Dong A, Wang Y, Gong J et al. FDG PET/CT findings of common bile duct tuberculosis. *Clin Nucl Med* 2014; 39: 67-70.
47. Sathekge M, Maes A, D'Asseler Y et al. Tuberculous lymphadenitis: FDG PET and CT findings in responsive and nonresponsive disease. *Eur J Nucl Med Mol Imaging* 2012; 39: 1184-90.
48. Fuster D, Tomas X, Mayoral M et al. Prospective comparison of whole-body ¹⁸F-FDG PET/CT and MRI of the spine in the diagnosis of haematogenous spondylodiscitis. *Eur J Nucl Med Mol Imaging* 2015; 42: 264-71.
49. Albano D, Treglia G, Desenzani P et al. Incidental Unilateral Tuberculous Sacroiliitis Detected by ¹⁸F-FDG PET/CT in a Patient with Abdominal Tuberculosis. *Asia Ocean J Nucl Med Biol* 2017; 5: 144-7.
50. Heysell SK, Thomas TA, Sifri CD et al. 18-Fluorodeoxyglucose positron emission tomography for tuberculosis diagnosis and management: a case series. *BMC Pulm Med* 2013; 13: 4.
51. Sathekge M, Maes A, Kgomo M et al. Impact of FDG PET on the management of TBC treatment. A pilot study. *Nuklearmedizin* 2010; 49: 35-40.
52. Vorster M, Sathekge MM, Bomanji J. Advances in imaging of tuberculosis: the role of ¹⁸F-FDG PET and PET/CT. *Curr Opin Pulm Med* 2014; 20: 287-93.
53. Lee IS, Lee JS, Kim SJ et al. Fluorine-18-fluorodeoxyglucose positron emission tomography/computed tomography imaging in pyogenic and tuberculous spondylitis: preliminary study. *J Comput Assist Tomogr* 2009; 33: 587-92.
54. Bassetti M, Merelli M, Di Gregorio F et al. Higher fluorine-18 fluorodeoxyglucose positron emission tomography (FDG-PET) uptake in tuberculous compared to bacterial spondylodiscitis. *Skeletal Radiol* 2017; 46: 777-83.
55. Dong A, Dong H, Wang Y et al. ¹⁸F-FDG PET/CT in differentiating acute tuberculous from idiopathic pericarditis: preliminary study. *Clin Nucl Med* 2013; 38: e160-5.
56. Abdul H, Abdul N, Nordin A. Dual time point imaging of FDG PET/CT in a tuberculous spondylodiscitis. *Biomed Imaging Interv J* 2010; 6: e18.
57. Xia Y, Qi C, Zhang S et al. Elevated ¹⁸F-NaF uptake in cricoid cartilage in a patient with laryngeal carcinoma: A case report and literature review. *Medicine* 2017; 96: e9090.
58. Sathekge M, Maes A, Van de Wiele C. FDG-PET imaging in HIV infection and tuberculosis. *Semin Nucl Med* 2013; 43: 349-66.
59. Rivas-Garcia A, Sarria-Estrada S, Torrents-Odin C et al. Imaging findings of Pott's disease. *Eur Spine J* 2013; 22 Suppl 4: 567-78.
60. Dureja S, Sen IB, Acharya S. Potential role of F-18 FDG PET-CT as an imaging biomarker for the noninvasive evaluation in uncomplicated skeletal tuberculosis: a prospective clinical observational study. *Eur Spine J* 2014; 23: 2449-54.
61. Chen RY, Dodd LE, Lee M et al. PET/CT imaging correlates with treatment outcome in patients with multidrug-resistant tuberculosis. *Sci Transl Med* 2014; 6: 265ra166.
62. Kimizuka Y, Ishii M, Murakami K et al. A case of skeletal tuberculosis and psoas abscess: disease activity evaluated using ¹⁸F-fluorodeoxyglucose positron emission tomography-computed tomography. *BMC Med Imaging* 2013; 13: 37.
63. Park IN, Ryu JS, Shim TS. Evaluation of therapeutic response of tuberculoma using F-18 FDG positron emission tomography. *Clin Nucl Med* 2008; 33: 1-3.
64. Martinez V, Castilla-Lievre MA, Guillet-Caruba C et al. ¹⁸F-FDG PET/CT in tuberculosis: an early non-invasive marker of therapeutic

- response. *Int J Tuberc Lung Dis* 2012; 16: 1180-5.
65. Kulshrestha RK, Vinjamuri S, England A et al. The Role of ^{18}F -Sodium Fluoride PET/CT Bone Scans in the Diagnosis of Metastatic Bone Disease from Breast and Prostate Cancer. *J Nucl Med Technol* 2016; 44: 217-22.
 66. Watanabe T, Takase-Minegishi K, Ihata A et al. ^{18}F -FDG and ^{18}F -NaF PET/CT demonstrate coupling of inflammation and accelerated bone turnover in rheumatoid arthritis. *Mod Rheumatol* 2016; 26: 180-7.
 67. Bastawrous S, Bhargava P, Behnia F et al. Newer PET application with an old tracer: role of ^{18}F -NaF skeletal PET/CT in oncologic practice. *Radiographics* 2014; 34: 1295-316.
 68. Bortot DC, Amorim BJ, Oki GC et al. ^{18}F -Fluoride PET/CT is highly effective for excluding bone metastases even in patients with equivocal bone scintigraphy. *Eur J Nucl Med Mol Imaging* 2012; 39: 17-30-6.
 69. Damle NA, Bal C, Bandopadhyaya GP et al. The role of ^{18}F -fluoride PET/CT in the detection of bone metastases in patients with breast, lung and prostate carcinoma: a comparison with FDG PET/CT and $^{99\text{mTc}}$ -MDP bone scan. *Jpn J Radiol* 2013; 31: 262-9
 70. Freesmeyer M, Stecker FF, Schierz JH et al. First experience with early dynamic ^{18}F -NaF-PET/CT in patients with chronic osteomyelitis. *Ann Nucl Med* 2014; 28: 314-21.
 71. Wong KK, Pierr M. Dynamic bone imaging with $^{99\text{mTc}}$ -labeled diphosphonates and ^{18}F -NaF: mechanisms and applications. *J Nucl Med* 2013; 54: 590-9.
 72. Langsteger W, Rezaee A, Pirich C et al. ^{18}F -NaF-PET/CT and $^{99\text{mTc}}$ -MDP Bone Scintigraphy in the Detection of Bone Metastases in Prostate Cancer. *Semin Nucl Med* 2016; 46: 491-501.
 73. D'Souza MM, Tripathi M, Shrivastav M et al. Tuberculosis mimicking malignancy. *Hell J Nucl Med* 2009; 12(1): 69-70.
 74. Ozmen O, Gokcek A, Tatci E et al. Integration of PET/CT in Current Diagnostic and Response Evaluation Methods in Patients with Tuberculosis. *Nucl Med Mol Imaging* 2014; 48: 75-8.
 75. Chong SG, Herron M, Dolan L et al. TB osteomyelitis. *QJM* 2016; 109: 751-2.
 76. Karkhur Y, Tiwari V, Lodhi J et al. Astragalus Tuberculosis: A Case Report and Review of the Literature. *Cureus* 2017; 9: e1708.
 77. Meena UK, Saibaba B, Behera P et al. Sternoclavicular joint tuberculosis: A series of 9 cases. *Indian J Tuberc* 2017; 64: 221-4.



Statets: Old Greek coins made of any kind of material. Its value was 2 drachmae. a) Head of the Sun in gold, 375b.C, found in Rhodes, b) Iraklis wrestling with a lion, 350-330b.C, found in the city of Irakleia, Italy